2015/08/08
Head Id: 299457
Archive Id: 299463P
Archive Date: 2015/08/08
Archive Tag: trunk

Measurement of top-quark polarisation in t-channel single top-quark production

The CMS Collaboration

Abstract

A measurement of the top-quark spin asymmetry, sensitive to the top quark polarisation, in t-channel single top-quark production ~~is presented~~, based on ~~approximately~~ 20 fb^{-1} of pp collisions at a centre-of-mass energy of 8 TeV. A high-purity sample of ~~t-channel~~ single top-quark events is selected, signal and background components ~~are~~ estimated using a fit to data ~~and an~~ unfolding technique is ~~applied~~ to measure the parton-level distribution of an angular observable sensitive to the top-quark polarisation. ~~The unfolded distribution is used to extract a top-quark~~ spin asymmetry ~~of~~ $A_\mu = 0.260 \pm 0.026(\text{stat.}) \pm 0.102(\text{syst.})$, which is compatible with the ~~SM prediction~~ of 0.438 ~~with a p-value of~~ 4.6%.

1 Introduction

The top quark is the heaviest elementary particle ~~discovered so far.~~ Its lifetime ($\tau \approx 4 \times 10^{-25}$ s) is much shorter than ~~the~~ typical quantum chromodynamics (QCD) ~~timescales~~. ~~Therefore, it is~~ the only quark that can decay (through electroweak interactions) before hadronising. Furthermore, the parity-violating nature of the electroweak interaction at the Wtb vertex ~~(V–A)~~ means that only left-handed quarks are expected ~~at this vertex. Thus, top quark~~ decay products ~~retain~~ memory of the ~~top quark~~ spin orientation in their angular distributions. This fact turns the top quark into a powerful tool to examine the structure of the ~~electroweak~~ Wtb vertex.

In electroweak single top-quark production ~~via~~ the t-channel, the ~~standard model (~~SM~~)~~ predicts that top quarks are produced $\approx 100\%$ polarized through the V–A coupling structure along the direction of the momentum of the spectator quark that recoils against the single top quark [1, 2]. ~~Equally, new physics models may~~ lead to a depolarisation in production or decay by altering the coupling structure [3–6].

Previously, ~~the measurement of~~ top-quark polarisation in single top-quark production has only been ~~performed~~ by the CDF collaboration [7]. However, with only 3.2 fb^{-1} of $\mathrm{p\bar{p}}$ collision data at a centre-of-mass energy of 1.96 TeV, the precision was not sufficient to exclude the ~~hypothesis~~ that single top quarks have ~~the~~ opposite polarisation to ~~the one predicted by~~ the SM ~~or are~~ produced unpolarised.

In this analysis, the top-quark spin asymmetry

$$A_{\mu} \equiv \frac{1}{2} \cdot P_t \cdot \alpha_{\mu} = \frac{N(\uparrow) - N(\downarrow)}{N(\uparrow) + N(\downarrow)} \tag{1}$$

is used to probe the ~~top quark~~ coupling structure. ~~In the above formula,~~ P_t represents the top-quark polarisation in production and α_X denotes the spin-analysing power of a decay product particle X, i.e. the degree of correlation of its angular distributions ~~with respect~~ to the spin of the top quark. The variables $N(\uparrow)$ and $N(\downarrow)$ are defined for each top-quark decay product from the ~~decay~~ chain $\mathrm{t} \to \mathrm{bW} \to \mathrm{b}\mu\nu$ as the number of instances in which that decay product is aligned or ~~counter-aligned with~~ the direction of the spectator quark momentum~~, respectively~~.

In this analysis, the muon is chosen as the ~~top quark spin~~ analyser because ~~of because~~ leptons have ~~the~~ highest spin-analysing power and because of the purity of ~~its~~ identification ~~with~~ the CMS detector. The spin-analysing power is exactly 1 at LO in the SM. Its value can be modified by anomalous top-quark couplings that would be characterised through an effective extension of the coupling structure of the Wtb production and decay vertices [5, 6].

An analysis of the top-quark spin asymmetry, measured in t-channel single top-quark events with one isolated muon in the final state, is ~~documented in~~ this paper.

The analysis strategy is ~~the following:~~ After applying an event selection designed to obtain a set of relatively high purity t-channel single-top quark events, the signal and background yields are estimated using a binned likelihood fit. A top quark candidate is reconstructed in whose rest frame the angle between the muon and the recoiling jet is calculated.

An unfolding technique is applied to extract the parton-level version of this angular distribution. From the unfolded distribution, the top-quark spin asymmetry, which is directly related to the polarisation through ~~equation 1~~, is calculated.

2 CMS detector

The central feature of the CMS apparatus is a superconducting solenoid of 6 m internal diameter, providing a magnetic field of 3.8 T. Within the superconducting solenoid volume are a silicon pixel and strip tracker, a lead tungstate crystal electromagnetic calorimeter (ECAL), and a brass and scintillator hadron calorimeter (HCAL), each composed of a barrel and two endcap sections. Muons are measured in gas-ionisation detectors embedded in the steel flux-return yoke outside the solenoid. Extensive forward calorimetry complements the coverage provided by the barrel and endcap detectors. A more detailed description of the CMS detector, together with a definition of the coordinate system ~~used~~ and ~~the~~ relevant kinematic variables, can be found in Ref. [8].

The particle-flow event algorithm [9, 10] reconstructs and identifies each individual particle with an optimized combination of information from the ~~various~~ elements of the CMS detector. The energy of photons is ~~directly~~ obtained from the ECAL measurement, corrected for ~~zero-suppression effects~~. The energy of electrons is determined from a combination of the electron momentum at the primary interaction vertex as determined ~~by~~ the tracker, the energy of the corresponding ECAL cluster, and the energy sum of all bremsstrahlung photons spatially compatible with originating from the electron track. The energy of muons is obtained from the curvature of the corresponding track. The energy of charged hadrons is determined from a combination of their momentum ~~measured~~ in the tracker and the matching ECAL and HCAL energy deposits, corrected for zero-suppression ~~effects~~ and for the response ~~function~~ of the calorimeters to hadronic showers. Finally, the energy of neutral hadrons is obtained from the corresponding corrected ECAL and HCAL energy. ~~In order to~~ mitigate the effect of pileup, i.e. additional proton-proton collisions whose signals in the detector sum to the products of the primary interaction that triggered the event, charged particles associated to non-leading primary vertices are vetoed.

The missing transverse momentum vector, $\vec{p}_{\mathrm{T}}^{\,\mathrm{miss}}$, is defined as the projection onto the plane perpendicular to the beams of the negative vector sum of the momenta of all reconstructed particles in an event. Its magnitude is referred to as $\not\!\!E_{\mathrm{T}}$.

3 Data and Simulated Samples

This study is based on the full data ~~set~~ recorded by the CMS detector [8] ~~in 2012~~ at a centre-of-mass energy of 8 TeV with an integrated luminosity of 19.7 ± 0.5 fb^{-1} [11].

Single top-quark t-channel events from Monte Carlo (MC) simulation used in this study have been generated with the next-to-leading order (NLO) MC generator POWHEG [12–14], interfaced to PYTHIA 6.4 [15] for the parton showering. The τ decays are modelled with TAUOLA [16]. The 5-flavour scheme (5FS) is used in the generation, i.e. b quarks are considered among the incoming particles. As an alternative NLO generator, used to assess the dependence of the analysis on the modelling of the signal, we use the aMC@NLO generator [17] interfaced to PYTHIA 8 [18], with the 4-flavour scheme (4FS), i.e. b quarks in the initial state are only produced via gluon splitting. The results are compared with the predictions from the aforementioned NLO generators and from COMPHEP [19], interfaced to PYTHIA 6, with a matching procedure between the leading-order diagrams of the 5FS and 4FS based on the p_{T} of the associated b quark [20]. To perform a test of the unfolding procedure, special samples have been generated with COMPHEP with anomalous values of the Wtb-vertex coupling.

Several SM processes are taken into account as background to the analysis. The POWHEG gen-

erator interfaced with PYTHIA is also used to model the single top-quark tW and s-channel background events. The $t\bar{t}$, W boson in association with jets (W+jets) and Drell-Yan in association with jets (Z/γ^*+jets) processes are generated with MADGRAPH interfaced with PYTHIA 6 whilst TAUOLA is used to simulate the τ decays. Up to three (four) additional partons are generated at matrix-element level in $t\bar{t}$ (W+jets and Z/γ^*+jets) events. A procedure implemented during the event generation and based on the so-called "MLM prescription" [21, 22] avoids double counting the jets generated by the matrix element and by the parton showering. An alternative sample of W+jets generated with SHERPA at NLO [23, 24] is used to improve the modelling of this background. Diboson production (WW, WZ, ZZ) is simulated using PYTHIA 6. QCD multi-jet events (i.e., events where the muon does not come from a leptonically decaying W boson) are modelled using statistically independent samples in data, as detailed in Sec. 6.1. Other special samples of signal and background have been generated with different generator parameters (e.g. top-quark mass, fragmentation/renormalisation scale, etc.) in order to estimate the corresponding systematic uncertainties.

All single top-quark processes are normalised to approximate next-to-next-to-leading order (NNLO) predictions [25] ($\sigma_{\mathrm{t-channel}} = 87.1$ pb, $\sigma_{\mathrm{s-channel}} = 5.55$ pb, $\sigma_{\mathrm{tW}} = 22.2$ pb). Top-quark pair production is normalised to a full NNLO prediction that includes soft gluon resummation to next-to-next-to-leading-log order, as calculated with the TOP++2.0 program [26] ($\sigma_{\mathrm{t\bar{t}}} = 252.9$ pb). The W+jets and Z/γ^*+jets cross sections are calculated at NNLO with FEWZ [27] ($\sigma_{\mathrm{W+jets}} = 37,509$ pb, $\sigma_{Z/\gamma^*\mathrm{+jets}} \cdot BR(\mathrm{Z}/\gamma^* \rightarrow 1^+1^-) = 3,504$ pb with a generator-level threshold of $m_{1^+1^-} > 50$ GeV). The diboson cross sections are calculated at NLO with MCFM 5.8 [28] ($\sigma_{WW} = 54.8$ pb, $\sigma_{WZ} = 33.2$ pb, $\sigma_{ZZ} = 8.1$ pb).

The effect of pileup is evaluated using a simulated sample of minimum bias events produced using PYTHIA 6, superimposed onto the events in the simulated samples described above, taking into account in-time and out-of-time pileup contributions. The events are then reweighted in order to reproduce the true pileup distribution that can be inferred from the data. The procedure is validated by comparing the number of observed primary vertices between data and simulation. All generated events undergo a full GEANT 4 [29] simulation of the detector response.

4 Event Selection

The study presented here focuses on the $\mathrm{t} \rightarrow \mathrm{bW} \rightarrow \mathrm{b}\mu\nu$ decay channel. Signal events are characterised by exactly one isolated muon and large $\not{E}_{\mathrm{T}}$ originating from the neutrino coming from the leptonic decay of the W-boson, as well as by one central b jet from the top-quark decay and an additional light-quark jet (j') from the hard scattering process, which is preferentially produced in the forward region. A second b jet produced in association with the top quark can be present in the detector as well, although it yields a softer p_{T} spectrum with respect to the b jet from top-quark decay. The event selection follows closely that used in the measurement of the production cross section in the same channel [30].

The trigger selection is based on the presence of at least one isolated muon with transverse momentum $p_{\mathrm{T}} > 24$ GeV and pseudorapidity $|\eta| < 2.1$.

The existence of exactly one isolated muon candidate originating from the leading primary vertex is required. Muon candidates are only accepted if they pass the following requirements: A transverse momentum, p_{T}, of at least 26 GeV, a pseudorapidity, η, with absolute value smaller than 2.1, quality and identification criteria optimized for the selection of prompt muons, and an isolation requirement. Isolation is defined as the sum of the transverse en-

ergies deposited by stable charged hadrons, photons and neutral hadrons in a cone of size $\Delta R = \sqrt{(\Delta\eta)^2 + (\Delta\phi)^2} = 0.4$ around the muon direction. In order to pass the isolation requirement, this value must be less than 12% of the transverse momentum of the muon. Events are rejected if an additional muon or an electron candidate is present. The selection requirements for these additional electrons/muons are as follows: loose quality, identification and isolation criteria, $p_{\mathrm{T}} > 10$ or 20 GeV in the muon or electron case, respectively, and $|\eta| < 2.5$.

Jets are reconstructed from the particle-flow objects, clustered using the anti-k_{t} algorithm [31, 32] with a size parameter of 0.5. The jet momentum is determined as the vectorial sum of all particle momenta in the jet, and is found from simulation to be within 5% to 10% of the true momentum over the whole p_{T} spectrum and detector acceptance. An offset correction is applied to jet energies to take into account the contribution from additional proton-proton interactions within the same bunch crossing. Additional selection criteria are applied to each event to remove spurious jet-like features originating from isolated noise patterns in certain HCAL regions. The analysis considers jets within $|\eta| < 4.5$ whose calibrated transverse energy is greater than 40 GeV. The event is accepted for further analysis only if at least two such jets are reconstructed and selected.

In order to reduce the large background from W+jets events, we apply a b-tagging algorithm based on a combination of secondary vertices and track-based lifetime information [33]. A tight selection is applied on the b-tagging discriminant, which corresponds to a light-jet mis-tagging rate of around 0.1% and an efficiency of around 50% for jets originating from true b quarks in our signal simulation. The b-tagging performance in simulation is corrected to better match the performance observed in data [33], using data-MC scale factors that depend on the p_{T} and η of the selected jets.

In order to classify signal and control regions, different event categories "Njet Mtag" are defined, where N is the number of selected jets (2 or 3) and M is the number of selected b-tagged jets (0 or 1 or 2). The "2jets 1tag" category defines the region used for signal extraction, whereas the other categories, enriched in background processes with different compositions, are used for the control samples discussed in Section 6. The "2jets 1tag" itself is further divided into a control region (CR) and a signal region (SR), depending on the value of a multivariate discriminant described later.

In the "2jets 1tag" category a top-quark candidate is reconstructed starting from the b-jet, the muon and the $\not\!\!E_{\mathrm{T}}$ with the procedure described in [34]. In the other categories, the jet with the highest value of the b-tagging discriminator is used for the top quark reconstruction.

QCD multi-jet events are suppressed by setting a threshold on the output of a dedicated boosted decision tree ($\mathrm{BDT_{QCD}}$), trained with the following input observables:

- the missing transverse ~~energy~~, $\not\!\!E_{\mathrm{T}}$;
- the mass of the top-quark candidate, $m_{\mu\nu\mathrm{b}}$;
- the pseudorapidity of the top-quark candidate, $|\eta_{\mu\nu\mathrm{b}}|$;
- the transverse momentum of the b-tagged jet, $p_{\mathrm{T}}^{\mathrm{b}}$;
- the event isotropy, defined as $(\mathcal{S}_{max} - \mathcal{S}_{min})/\mathcal{S}_{max}$, where $\mathcal{S} \equiv \sum_{i \in \{\mu, jets\}} |\vec{P}_i|$ and $\vec{n}$ is a unit vector in the $r - \phi$ plane.

~~In order to further~~ reject background events, a second boosted decision tree, $\mathrm{BDT}_{W,t\bar{t}}$, ~~was~~ used to separate signal from $t\bar{t}$ and W+jets events. Training ~~was~~ performed with the following input observables:

- the mass of the top-quark candidate, $m_{\mu\nu \mathrm{b}}$;
- the pseudorapidity of the jet with smallest value of the b-tagging discriminator, $|\eta_{j'}|$;
- the pseudorapidity of the b-tagged jet, $|\eta_{\mathrm{b}}|$;
- the mass of the b-tagged jet, m_{b};
- the transverse momentum of the muon, p_{T}^{μ};
- the transverse energy of the b-tagged jet, $p_{\mathrm{T}}^{\mathrm{b}}$;
- the transverse W-boson mass, $m_{\mathrm{T}}(W) = \sqrt{\left(p_T^{\mu} + \not{E}_{\mathrm{T}}\right)^2 - \left(p_x^{\mu} + \not{E}_{\mathrm{T},x}\right)^2 - \left(p_y^{\mu} + \not{E}_{\mathrm{T},y}\right)^2}$;
- the missing transverse energy, $\not{E}_{\mathrm{T}}$;
- the total invariant mass of the top-quark candidate and the light-quark system, $\hat{S}$;
- the transverse momentum of the hadronic final state system, $H_T = \left(\vec{p}_{\mathrm{b}} + \vec{p}_{j'}\right)_{\mathrm{T}}$.

The BDT~~$_{\mathrm{QCD}}$~~ discriminant distribution is shown in two control regions in Fig. 1 for data and simulation, with the ~~QCD multi-jet shape~~ and normalization extracted as described in Sec. 6.1. Input variables ~~have been individually~~ validated in the same way. Figure 2 shows the distribution of the BDT$_{W,\mathrm{t\bar{t}}}$ discriminant in the "2jets 1tag" and "3jets 2tag" categories.

To select a signal-enhanced phase space, an additional selection on the discriminant ~~is imposed~~. The optimal working point is found to be BDT$_{W,\mathrm{t\bar{t}}} > 0.45$ by studying the analysis sensitivity with pseudo-data from simulated events ~~only~~.

All BDT input variables ~~have been~~ shown to be well modelled by the MC simulation. The BDT ~~was~~ trained and tested on statistically independent samples ~~and~~ no over-training ~~was~~ observed.

Corrections are applied to the simulation, where necessary, in order to account for known differences ~~with respect~~ to data. Single-muon trigger efficiencies and lepton reconstruction and identification efficiencies are estimated with a "tag and probe" method from Drell–Yan data [35], b-tagging and misidentification efficiencies are estimated from dedicated analyses performed with orthogonal selections [33] and a smearing is applied to account for the known difference in jet energy resolution compared to data [36]. All these corrections are found to be small.

5 The $\cos\theta^*_{\mu}$ Distribution of Top-Quark Decay Products

The angle between a top-quark decay product X $(= W, \ell, \nu, b)$ and an arbitrary polarisation axis S in the top-quark rest frame, θ^*_X, has a distribution ~~that is determined~~ according to the following differential cross section:

$$\frac{1}{\sigma}\frac{\mathrm{d}\sigma}{\mathrm{d}\cos\theta^*_X} = \frac{1}{2}(1 + P_t^{(S)}\alpha_X \cos\theta^*_X) = \left(\frac{1}{2} + A_X \cos\theta^*_X\right). \quad (2)$$

The variable $P_t^{(S)}$ denotes the single top-quark polarisation along the chosen axis and α_X the spin-analysing power as defined in ~~Sec.~~ 1. In the SM, the top-quark spin tends to be aligned with the direction of the spectator quark momentum, resulting in a high degree of polarisation. Hence, an excess of events where the spectator quark momentum is ~~counter~~ aligned with the top-quark spin would clearly indicate an anomalous coupling structure. Single top-quark polarisation is studied in the t-channel process through the angular asymmetry, A_{μ}, of the muon, where the polarisation axis is defined as pointing along the untagged jet (j') direction in the top quark rest frame.

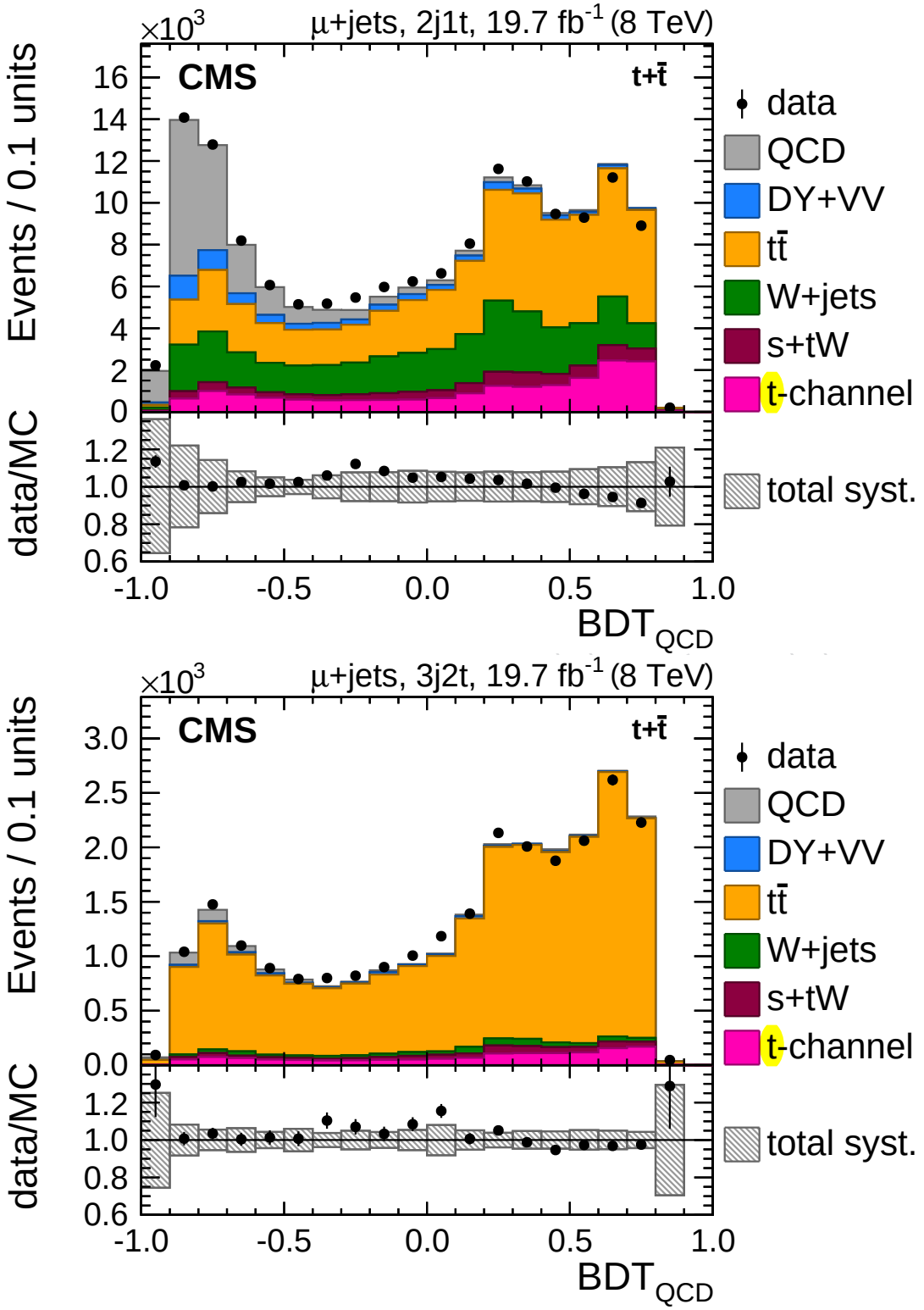

Figure 1: Distribution of the $\mathrm{BDT_{QCD}}$ discriminant in the "2jets 1tag" (top) and "3jets 2tag" (bottom) categories. Predictions are normalised to the results of the fit described in Sec. 7. The bottom panel in both figures shows the ratio between observed and predicted event counts, with a shaded area to indicate the systematic uncertainties affecting the background prediction.

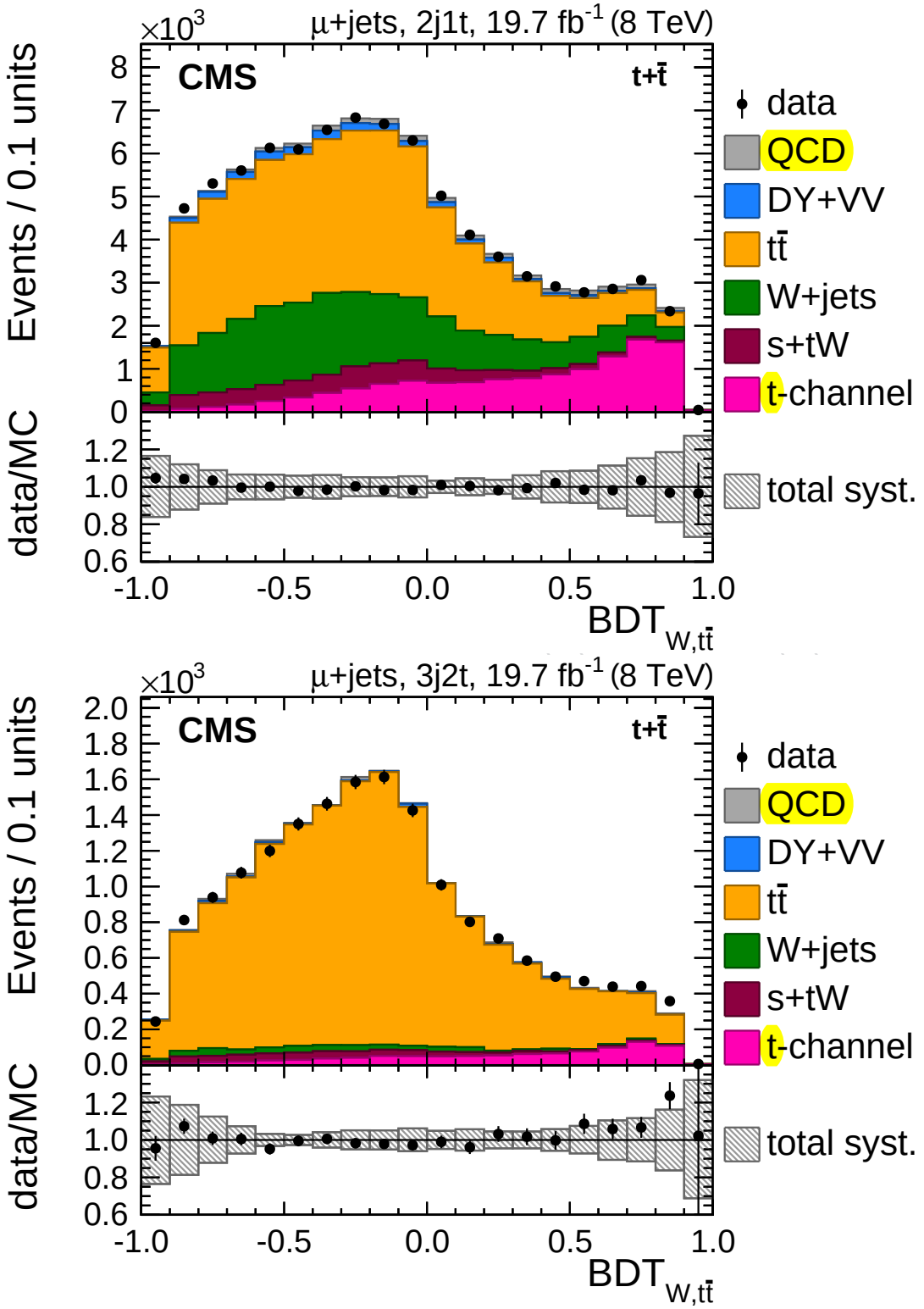

Figure 2: $\mathrm{BDT}_{W,t\bar{t}}$ discriminant distribution in the "2jets 1tag" category (top) and in the "3jets 2tag" control region (bottom). Predictions are normalised to the results of the fit described in Sec. 7. The bottom panel in both figures shows the ratio between observed and predicted event counts, with a shaded area to indicate the systematic uncertainties affecting the background prediction.

In this analysis, a χ^2-fit of the unfolded differential cross section based on equation 2 is used to estimate A_μ.

Figure 3 shows the reconstructed distribution of $\cos\theta^*_\mu$ in the "2jets 1tag" (for $\mathrm{BDT}_{W,\mathrm{t\bar{t}}} > 0.45$) and "3jets 2tag" categories.

6 Background Model Studies

Orthogonal control samples are used for several purposes in this analysis. Samples in which the isolation requirement on the muon has been inverted are used to extract templates for estimating the contamination by QCD multi-jet events, while samples with different jet and b-tagging multiplicities are used to validate the MC simulation of W+jets and $\mathrm{t\bar{t}}$ events or to provide additional constraints on the in situ determination of background and signal strengths.

6.1 QCD Multi-Jet Background Estimation

The yield of the QCD multi-jet background in the different categories is measured by performing fits to the $\mathrm{BDT}_{\mathrm{QCD}}$ discriminant distributions for each "Njet Mtag" category where a significant contamination from this process is expected. A binned maximum-likelihood (ML) template fit is performed, with two components: QCD multi-jet (unconstrained) and the sum of all other processes (log-normal constraint within $\pm 20\%$ of the expected yield). The latter category includes our signal. The templates for the sum of the non-QCD processes are taken from simulation, while the QCD multi-jet template is extracted from an orthogonal QCD-enriched sample in data defined by using the inverted-isolation QCD-enriched data sample defined above. It was verified that the $\mathrm{BDT}_{\mathrm{QCD}}$ discriminant distributions for QCD multi-jet events are not significantly affected by this altered event selection.

The relative uncertainties on the QCD multi-jet yield estimates are taken conservatively to be $\pm 50\%$ in addition to the shape variations observed when changing the range of the inverted isolation requirement. Together, these are used to estimate the systematic uncertainty associated with this procedure, as discussed in Section 9.

6.2 W+jets Model Validation and Correction

After the QCD multi-jet contribution to the signal region has been estimated, the agreement between the expectations and the data is verified in several control regions for all the $\mathrm{BDT}_{W,\mathrm{t\bar{t}}}$ inputs, for the $\mathrm{BDT}_{W,\mathrm{t\bar{t}}}$ response itself, for $\cos\theta^*_\mu$ and various additional variables. Among all the control regions considered, mismodellings in $\cos\theta^*_\mu$ and p_{T} of the reconstructed W-boson ($p_{\mathrm{T}}^{\mathrm{W}}$) are observed in the "2jets 0tags" control region; this region is expected to be enriched in W+jets events.

A similar disagreement between data and MADGRAPH expectations in the $\cos\theta^*_\mu$ distribution was observed in $\sqrt{s} = 7$ TeV data in the context of a different analysis [30]. Investigations using different MC generators and their associated settings showed that SHERPA [37] provided a better description of $\cos\theta^*_\mu$ in this control region at both centre-of-mass energies.

Although this control region is not used in the fit, more investigation has been performed in order to understand if this mismodelling can potentially affect the signal region. The MADGRAPH and SHERPA samples were found to differ mostly in the $\cos\theta^*_\mu$ distribution for events with a W produced in association with jets from gluon fragmentation, which constitutes a major component of the "2jets 0tags" region but is a very small fraction of the "2jets 1tag" signal region.

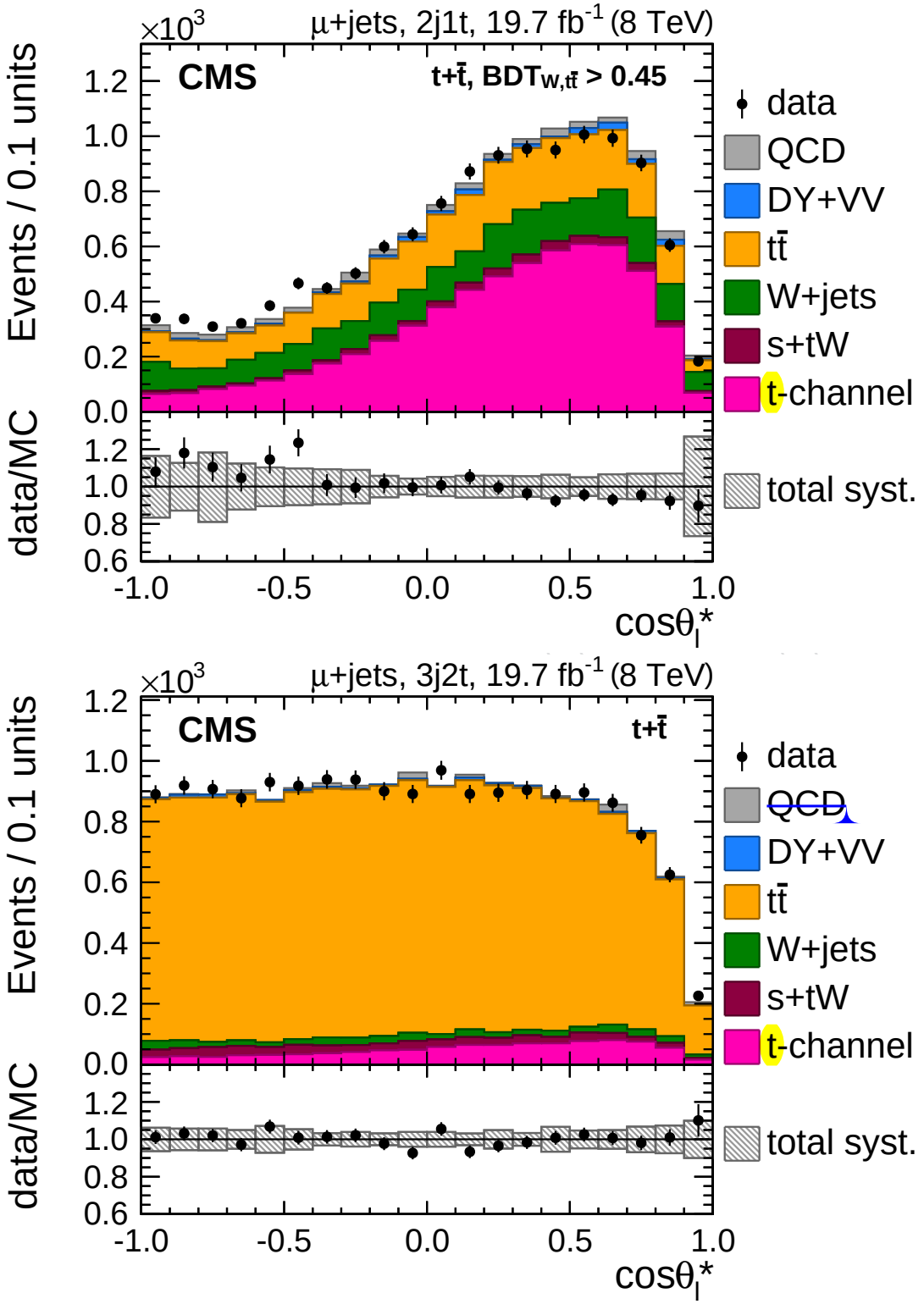

Figure 3: Distribution of $\cos\theta^*_\mu$ in the signal region defined by $\mathrm{BDT}_{W,t\bar{t}} > 0.45$ in the "2jets 1tag" category (top) and in the "3jets 2tag" control region (bottom). Predictions are normalised to the results of the fit described in Sec. 7. The bottom panel in both figures shows the ratio between observed and predicted event counts, with a shaded area to indicate the systematic uncertainties affecting the background prediction.

In the kinematic region sampled by this analysis, MADGRAPH reproduces the W+jets kinematic properties better than SHERPA. Moreover, for computational reasons the approximation $m_b = m_c = 0$ was used in the generation of the SHERPA samples, causing the relative fraction of heavy quarks to be unrealistically large. For these reasons MADGRAPH has been used as default generator in this analysis, and a reweighting of the W+jets events simulated with MADGRAPH has been performed in all signal and control regions by using the event ratio between the two generators as a function of $\cos\theta^*_\mu$, separately for each flavour component in the "2jets 0tags" control region. It has been verified at the generator level that the kinematic properties of the W+jets events, including the $\cos\theta^*_\mu$ distribution, are not significantly affected by the treatment of the b and c quark masses.

6.3 $t\bar{t}$ Model Validation

In order to validate the $t\bar{t}$ simulation, this is compared to data in the "3jets 2tags" control region for the most relevant observables. In particular, the right-hand panels of figures 1, 2 and 3 show the BDT_{QCD} and $BDT_{W,t\bar{t}}$ discriminants and $\cos\theta^*_\mu$ distributions, respectively. This control region is also used in the fit described in Sec. 7.

The MADGRAPH model of $t\bar{t}$ production is known to predict a harder top-quark p_T spectrum than observed in data [38, 39]; we therefore reweight the spectrum of generator-level top quarks in $t\bar{t}$ events such that it reproduces the measured differential cross section with respect to top quark transverse momentum.

In conclusion, the $t\bar{t}$ modelling provided by MADGRAPH is found to be in reasonable agreement with data.

7 The Extraction of Signal and Background Yields

We estimate the signal and background components by means of a simultaneous maximum likelihood fit based on the ~~shape of~~ the $BDT_{W,t\bar{t}}$ discriminant in the "2jets 1tag" and "3jets 2tags" regions.

For all background processes, except the QCD multi-jet background, we use the templates derived from the MC samples. The QCD multi-jet template is derived directly from data by inverting some of the event selection cuts, as described earlier, and its normalisation is kept fixed to the estimation described in Sec. 6.1. In order to reduce the number of free parameters, several processes that have a similar shape in both $\cos\theta^*_\mu$ and the $BDT_{W,t\bar{t}}$ discriminant are merged into a single template:

- Signal: t-channel single top-quark production, treated as unconstrained.
- Top-like processes: $t\bar{t}$, s-channel and W-associated (tW) single top-quark production, with their relative fractions taken from simulation; we consider a $\pm 20\%$ log-normal constraint.
- W/Z+jets: W+jets, Z/γ^*+jets and diboson (WW, WZ, ZZ) production with their relative fractions taken from simulation; we apply a $\pm 50\%$ log-normal constraint.

The results of the fit and the post-fit uncertainties are presented in Table 1, while Table 2 shows the number of events exceeding the threshold on the $BDT_{W,t\bar{t}} > 0.45$ discriminant, normalised to the fit results.

Processes	Top	Antitop	Top and antitop
Signal	1.10 ± 0.03	1.20 ± 0.05	1.13 ± 0.03
Top	1.06 ± 0.02	1.08 ± 0.02	1.07 ± 0.01
EW	1.26 ± 0.05	1.21 ± 0.06	1.24 ± 0.04

Table 1: Estimated scale factors and uncertainties from the simultaneous ML-fit to the shape of the $\mathrm{BDT}_{W,\mathrm{t\bar{t}}}$ discriminant in the "2jets 1tag" and "3jets 2tag" categories.

Process	Top	Antitop	Top and antitop
$\mathrm{t\bar{t}}$	1543 ± 24	1573 ± 23	3118 ± 34
tW	143 ± 8	168 ± 9	311 ± 12
s-channel	44 ± 4	27 ± 3	72 ± 4
W+jets	1332 ± 60	1022 ± 56	2353 ± 81
DY-jets	181 ± 23	189 ± 23	371 ± 32
Diboson	21 ± 2	13 ± 1	33 ± 2
QCD	219 ± 110	208 ± 105	427 ± 214
t-channel	3852 ± 101	2202 ± 90	6049 ± 136
Total Expected	7334 ± 165	5402 ± 153	12733 ± 271
Data	7223 ± 85	5281 ± 73	12504 ± 112

Table 2: The expected number of signal and background events in the "2jets 1tag" region after the threshold requirement on the $\mathrm{BDT}_{W,\mathrm{t\bar{t}}}$ discriminant and applying the ML-fit result. The uncertainties reflect the limited MC statistics and residual fitting uncertainty where appropriate. The QCD multi-jet background contribution is estimated using a data-driven procedure.

8 Unfolding

An unfolding procedure is used to extract the $\cos\theta^*_\mu$ distribution at parton level. It accounts for distortions coming from the detector acceptance, selection efficiencies, imperfect reconstruction of the top-quark candidate, and the approximation made in treating the direction of the untagged jet as the spin axis.

In simulation, the parton-level definition of $\cos\theta^*_\mu$ is built by using the generated muon coming from the decay chain of a top or antitop quark and the light quark scattering off the top or antitop quark by virtual W-boson exchange, and boosting all objects into the rest frame of the generated top or antitop quark. In order to preserve the spin information from the W decay, the response matrix takes into account the case in which the muon comes from a τ decay by unfolding to the level of the τ lepton.

Prior to unfolding, remaining background constributions are subtracted from the reconstructed data distribution for which the fitted numbers of events and their uncertainties, estimated in Section 7, are used.

After the background subtraction, an unfolding procedure [40] is applied. Its core is the application of a matrix inversion using second derivatives for regularisation. A detailed description of the procedure can be found in the $\mathrm{t\bar{t}}$ charge asymmetry analysis [41] performed previously by CMS, which utilises the same method.

The performance of the unfolding algorithm is tested in sets of pseudo-experiments. An examination of the pull distribution has shown that the uncertainties have been treated correctly. A closure test was performed by injecting anomalous Wtb-vertex couplings as pseudo-data, which were generated with COMPHEP [19, 20]. This test verified that, with this analysis strat-

egy, it is possible to measure different asymmetries correctly with minimal bias.

The value of A_μ is extracted using a χ^2-fit of the unfolded $\cos\theta^*_\mu$ distribution, under the assumption that equation 2 is valid. The fit takes into account the bin-by-bin correlations that are induced by the unfolding procedure.

An alternative procedure has been used as a cross check, based on analytical matrix inversion with only two bins in the $\cos\theta^*_\mu$ distribution (corresponding to forward- and backward-going charged leptons). Although the results of the two methods are in agreement, the precision of the analytical matrix inversion is slightly worse.

9 Systematic Uncertainties

The measurement presented in this paper will potentially be affected by several sources of systematic uncertainty. To evaluate the impact of each source, we perform a new background estimation and repeat the measurement on data using systematically shifted simulated templates and response matrices. The expected systematic uncertainty for each source is taken to be the maximal shift in the values of the asymmetry between the nominal asymmetry and the one measured using the shifted templates.

Limited number of simulated events: The uncertainty associated with the limited amount of simulated events used in the templates is taken into account at all stages of the analysis, i.e. both in terms of fluctuations in the background templates and in determining the elements of the migration matrix.

ML-fit uncertainty: This uncertainty is determined by propagating the uncertainty associated with the background normalisation coming from the maximum likelihood fit through the remainder of the analysis, ensuring that the correlations between bins are taken into account.

Generator model: The nominal result is compared with the one obtained using an unfolding matrix derived from a signal sample generated with aMC@NLO, interfaced to PYTHIA 8 for the parton showering, and using the same settings as the main sample.

Parton distribution functions: The uncertainty due to the choice of the set of parton distribution functions (PDF) is estimated by reweighting the simulated events with each of the 52 eigenvectors of the CT10 collection [42], plus the best-fit sets from the MSTW2008CPDEUT [43] and NNPDF23 [44] collections. The unfolding procedure is repeated for each of these 54 cases. For the reweighting of the simulated events, the LHAPDF [45] package is used.

Renormalisation and factorisation scale uncertainty: The uncertainties on the renormalisation and factorisation scales (set in our simulation to a common scale, Q) are evaluated for signal, $\mathrm{t\bar{t}}$ and W+jets independently, by doubling or halving the value.

For signal, a re-weighting procedure is applied to simulated events based on the scale dependence of the matrix element generation and neglecting the corresponding dependence of the parton shower. Since the signal process does not contain a QCD vertex at LO, its scale dependence through the matrix element with scale Q can be approximated by

$$\mathrm{ME}(Q) \propto \mathrm{PDF}(x_1, Q) \cdot \mathrm{PDF}(x_2, Q) \tag{3}$$

where x_i are the momentum fractions of the two partons from the colliding protons. An event weight is then defined as:

$$w(Q \to Q')^{\text{ME-only}} = \frac{\mathrm{PDF}(x_1, Q') \cdot \mathrm{PDF}(x_2, Q')}{\mathrm{PDF}(x_1, Q) \cdot \mathrm{PDF}(x_2, Q)}. \tag{4}$$

Dedicated simulated samples with doubled and halved scales have been used to verify the validity of the approximation of ignoring the scale effect on the parton shower simulation for the signal process. The reweighting is preferred over the usage of the dedicated samples because of their limited amount of events.

For the $t\bar{t}$ and W+jets backgrounds, a looser threshold is applied to the $BDT_{W,t\bar{t}}$ discriminant in the simulated samples in which the scale has been varied. This is done to enhance the number of events available in these samples. This method provides an extracted $\cos\theta^*_\mu$ shape that agrees within the limited number of simulated events when applying the nominal $BDT_{W,t\bar{t}}$ discriminant threshold to those samples instead.

Top-quark mass uncertainty: Additional $t\bar{t}$ and signal simulation samples have been produced with the top-quark mass varied by ± 3 GeV. These samples are used to determine the uncertainty arising from our knowledge of the top-quark mass. This is a conservative estimate as the current world average is 173.3 ± 0.8 GeV [46].

W+jets p_T reweighting: The MADGRAPH model of W+jets predicts a different p_T^W spectrum from data observed in the "2 jets 0 tags" control region. We reweight the distribution to data (after subtraction of other processes) and take the difference as a systematic uncertainty.

W+jets background modelling: An uncertainty of the fraction of W+jets events in which the jets arise from heavy flavours is taken into account by scaling its contribution by $\pm 50\%$ with respect to the MADGRAPH expectation. The uncertainty associated to the reweighting procedure presented in Section 6.2 is estimated conservatively by comparing the result after reweighting with that determined with no weighting applied. The difference between the two is then symmetrised.

$t\bar{t}$ background modelling (top p_T reweighting): The MADGRAPH model of $t\bar{t}$ production is known to predict a harder p_T^t spectrum compared to that observed in the data [38, 39]. Although the correlation with other uncertainty sources is not clear yet, we reweight the spectrum of generator-level top quarks in $t\bar{t}$ events to the measured differential cross section in the analysis and apply an additional systematic on this reweighting by doubling and negating the reweighting.

ME-PS matching threshold uncertainty: The effect of the matching threshold between Matrix Element and Parton Shower in the MLM procedure is evaluated for $t\bar{t}$ and W+jets, independently, using dedicated samples in which the threshold is either doubled or halved.

Muon trigger, identification and isolation efficiencies: A systematic uncertainty of 1% is applied independently to the muon trigger, muon identification and muon isolation efficiencies. These uncertainties are found to cover the different efficiencies between the phase space regions sampled by our selection and by the one applied to select Z/γ^*+jets events for the "tag and probe" extraction.

Detector-related jet and $\not{E}_T$ effects: All reconstructed jet four-momenta in simulated events are simultaneously varied according to the η and p_T-dependent uncertainties on the jet energy scale [36]. This variation in jet four-momenta is also propagated to $\not{E}_T$. In addition, the effect on the measurement of $\not{E}_T$ arising from the 10% uncertainty associated with the unclustered energy deposits in the calorimeters is estimated after subtracting from $\not{E}_T$ all jets and leptons. The extra resolution contribution applied to account for the known difference with respect to data [36] is increased or decreased by its uncertainty.

b-tagging: The uncertainties on the tagging and mistagging efficiencies for individual jets as measured from data [33] are propagated to the event weights in simulation.

Pileup: A 5% uncertainty is applied to the average expected number of pileup interactions in order to estimate the uncertainty arising from the modelling of pileup.

QCD multi-jet yield: A 50% uncertainty is assigned to the yield obtained from the QCD multi-jet fit.

QCD multi-jet template: A shape uncertainty is taken into account by varying the anti-isolation range used to extract the templates used to estimate this background contribution.

Other background fractions: A specific uncertainty is assigned to the fraction of each minor process that is combined with similar and larger processes in the fit. These are dibosons and Z/γ^*+jets for the W/Z+jets component and the single-top tW and s-channel for the top quark component. The uncertainty on the yield is 50% for each of the templates.

Unfolding bias: A closure test of the analysis strategy has shown a small bias when injecting anomalous couplings samples with various different asymmetries as pseudo-data. We treat this as an additional systematic uncertainty on the asymmetry measurement only.

Table 3 shows the impact of the different sources of systematic uncertainties on the asymmetry measurements.

10 Results

Figures 4 and 5 show the results of the unfolding procedure for single top and single antitop production and for their combination, showing statistical and total uncertainties, with a comparison to the SM expectations, as predicted by POWHEG, aMC@NLO, and COMPHEP. Uncertainties arising from Q^2-scale and PDF variations have been found negligible on the predicted differential distributions and are therefore not shown.

The asymmetry, A_μ, is extracted from the the unfolded cross section according to ~~equation 1,~~ taking into account correlations. Using this procedure, we obtain:

$$A_\mu(t) = \Big[29.0 \pm 3.2(\text{stat.}) \pm 10.0(\text{syst.})\Big] \times 10^{-2} = \Big[29.0 \pm 10.5\Big] \times 10^{-2}, \quad (5)$$

$$A_\mu(\bar{t}) = \Big[21.1 \pm 4.6(\text{stat.}) \pm 12.6(\text{syst.})\Big] \times 10^{-2} = \Big[21.1 \pm 13.8\Big] \times 10^{-2}, \quad (6)$$

$$A_\mu(t+\bar{t}) = \Big[26.0 \pm 2.6(\text{stat.}) \pm 10.2(\text{syst.})\Big] \times 10^{-2} = \Big[26.0 \pm 10.5\Big] \times 10^{-2} \quad (7)$$

where the combined result is compatible with a p-value of $p(\text{data}|\text{SM}) = 4.6 \times 10^{-2}$ that corresponds to a difference of 1.7 standard deviations compared to the expected SM asymmetry of 43.8×10^{-2} as predicted by POWHEG.

As a cross-check, we also perform an analytical 2-bin unfolding, which directly yields the numbers $N(\uparrow)$ and $N(\downarrow)$ (see equation 1). This results in a value for A_μ of:

$$A_\mu(t+\bar{t}) = \Big[27.6 \pm 3.1(\text{stat.}) \pm 11.1(\text{syst.})\Big] \times 10^{-2} = \Big[27.6 \pm 11.5\Big] \times 10^{-2}. \quad (8)$$

11 Summary

The first measurement of the top-quark spin asymmetry (which is sensitive to the top quark polarisation) in t-channel single-top-production has been presented, based on approximately

	$\delta A_\mu(t) \times 10^2$	$\delta A_\mu(\bar{t}) \times 10^2$	$\delta A_\mu(t+\bar{t}) \times 10^2$
statistical	3.2	4.6	2.6
ML-fit uncertainty	0.7	1.2	0.6
Diboson fraction	< 0.1	< 0.1	< 0.1
Drell-Yan fraction	< 0.1	< 0.1	< 0.1
s-channel fraction	0.3	0.2	0.2
tW fraction	0.1	0.7	0.2
~~QCD shape~~	0.5	0.7	0.5
~~QCD yield~~	1.9	1.2	1.7
b tagging	0.7	1.2	0.9
mistagging	< 0.1	0.1	< 0.1
JER	2.7	1.8	2.0
JES	1.3	2.6	1.1
unclustered $\not{E}_T$	1.1	3.3	1.3
pileup	0.3	0.2	0.2
lepton ID	< 0.1	< 0.1	< 0.1
lepton isolation	< 0.1	< 0.1	< 0.1
trigger efficiency	< 0.1	< 0.1	< 0.1
top p_T reweighting	0.3	0.3	0.3
W+jets W p_T reweighting	0.1	0.1	0.1
W+jets heavy flavour fraction	4.7	6.2	5.3
W+jets light flavour fraction	< 0.1	< 0.1	0.1
W+jets shape reweighting	2.9	3.4	3.1
unfolding bias	2.5	4.2	3.1
generator model	1.6	3.5	0.3
top quark mass	1.9	2.9	1.8
PDF	0.9	1.6	1.2
Q^2 scale t-channel	0.2	0.2	0.2
$t\bar{t}$ Q^2 scale	2.2	3.4	2.7
$t\bar{t}$ matching	2.2	0.5	1.6
W+jets Q^2 scale	3.7	4.6	4.0
W+jets matching	3.8	3.0	3.4
limited MC	2.1	3.2	1.8
total uncertainty	10.5	13.8	10.5

Table 3: List of systematic uncertainties and their induced shift from the nominal measuremed asymmetry for the top ($\delta A_\mu(t)$), antitop ($\delta A_\mu(\bar{t})$), and their combination ($\delta A_\mu(t+\bar{t})$).

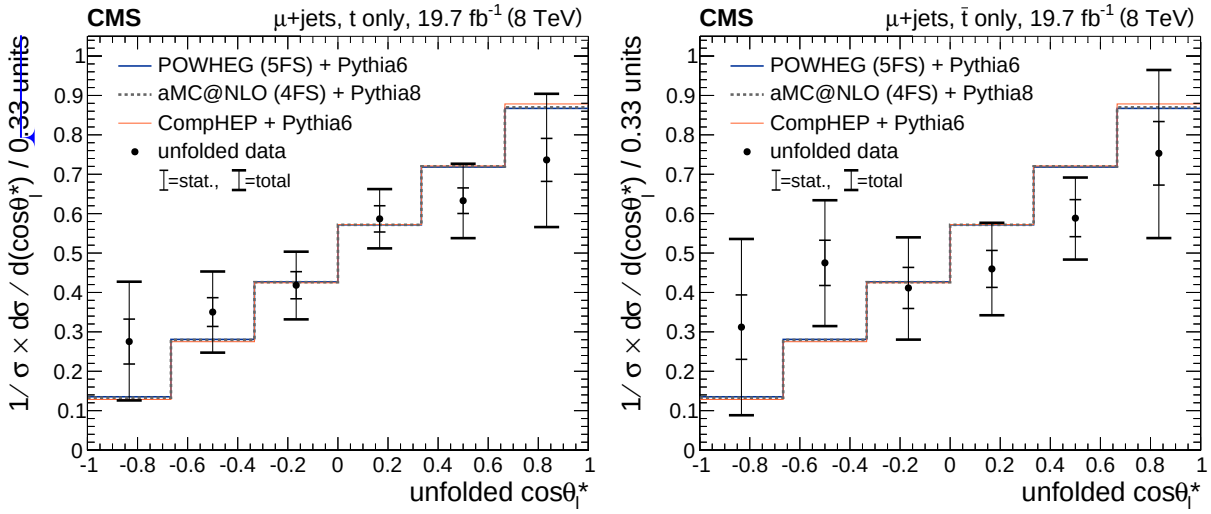

Figure 4: The normalised differential cross section ~~with respect to~~ $\cos\theta^*_{\text{unfolded}}$ for top (left) and antitop (right) compared to the predictions from POWHEG, aMC@NLO, and CompHEP. ~~Error bars~~ represent statistical and total uncertainties.

~~20~~ fb^{-1} of pp collisions at a centre-of-mass energy of 8 TeV.

The $\cos\theta^*_{\text{unfolded}}$ distribution displays a ~~difference~~ of 1.7 ~~compared to~~ the SM expectation, which is not statistically significant.

The asymmetry between forward- and backward-going charged leptons ~~with respect~~ to the direction of the untagged jets in the top-quark rest frame is measured to be $A_\mu = \left[26.0 \pm 2.6(\text{stat.}) \pm 10.2(\text{syst.})\right] \times 10^{-2} = \left[26.0 \pm 10.5\right] \times 10^{-2}$.

Acknowledgements

We congratulate our colleagues in the CERN accelerator departments for the excellent performance of the LHC and thank the technical and administrative staffs at CERN and at other CMS institutes for their contributions to the success of the CMS effort. In addition, we gratefully acknowledge the computing centres and personnel of the Worldwide LHC Computing Grid for delivering so effectively the computing infrastructure essential to our analyses. Finally, we acknowledge the enduring support for the construction and operation of the LHC and the CMS detector provided by the following funding agencies: the Austrian Federal Ministry of Science and Research and the Austrian Science Fund; the Belgian Fonds de la Recherche Scientifique, and Fonds voor Wetenschappelijk Onderzoek; the Brazilian Funding Agencies (CNPq, CAPES, FAPERJ, and FAPESP); the Bulgarian Ministry of Education and Science; CERN; the Chinese Academy of Sciences, Ministry of Science and Technology, and National Natural Science Foundation of China; the Colombian Funding Agency (COLCIENCIAS); the Croatian Ministry of Science, Education and Sport, and the Croatian Science Foundation; the Research Promotion Foundation, Cyprus; the Ministry of Education and Research, Recurrent financing contract SF0690030s09 and European Regional Development Fund, Estonia; the Academy of Finland, Finnish Ministry of Education and Culture, and Helsinki Institute of Physics; the Institut National de Physique Nucléaire et de Physique des Particules / CNRS, and Commissariat à l'Énergie Atomique et aux Énergies Alternatives / CEA, France; the Bundesministerium für Bildung und Forschung, Deutsche Forschungsgemeinschaft, and Helmholtz-Gemeinschaft Deutscher Forschungszentren, Germany; the General Secretariat for Research and Technology,

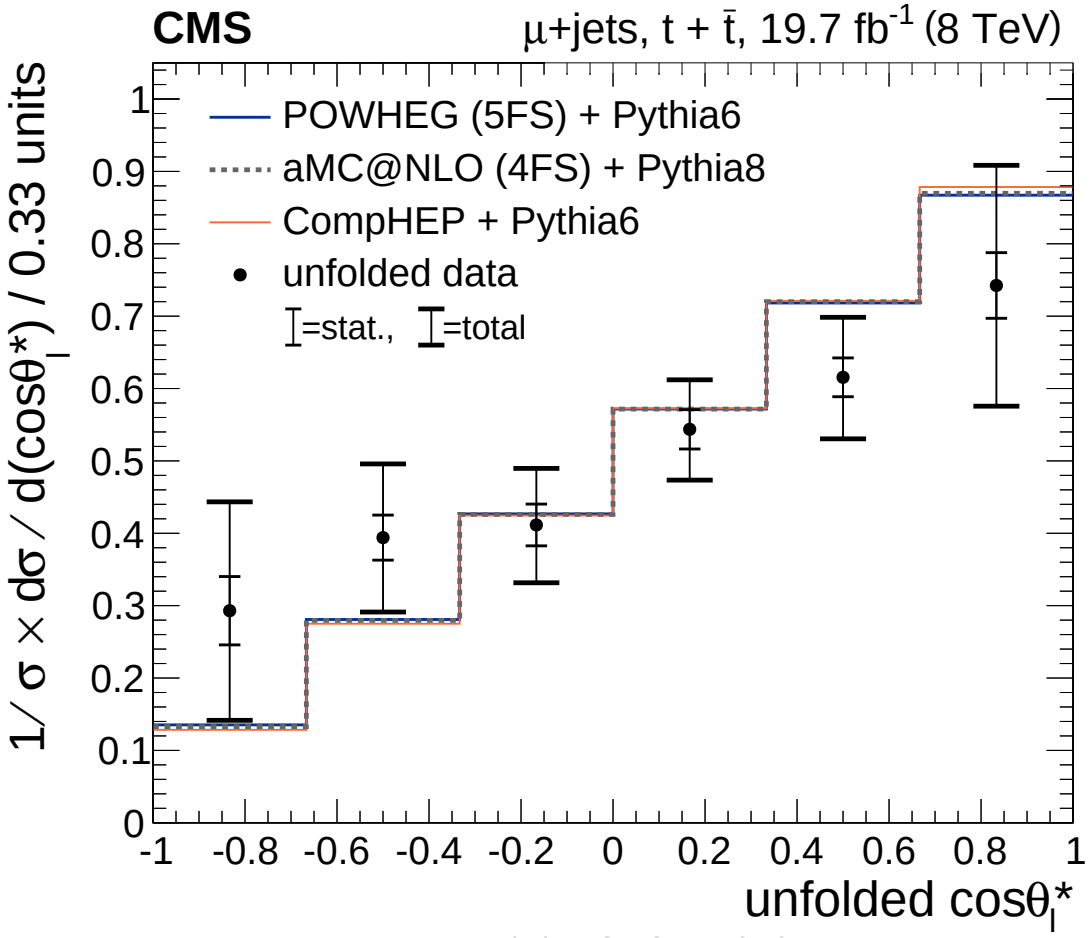

Figure 5: The normalised differential cross section with respect to $\cos\theta^*_{\text{unfolded}}$ for top and antitop combined compared to the predictions from POWHEG, aMC@NLO, and CompHEP. Error bars represent statistical and total uncertainties.

Greece; the National Scientific Research Foundation, and National Innovation Office, Hungary; the Department of Atomic Energy and the Department of Science and Technology, India; the Institute for Studies in Theoretical Physics and Mathematics, Iran; the Science Foundation, Ireland; the Istituto Nazionale di Fisica Nucleare, Italy; the Korean Ministry of Education, Science and Technology and the World Class University program of NRF, Republic of Korea; the Lithuanian Academy of Sciences; the Ministry of Education, and University of Malaya (Malaysia); the Mexican Funding Agencies (CINVESTAV, CONACYT, SEP, and UASLP-FAI); the Ministry of Business, Innovation and Employment, New Zealand; the Pakistan Atomic Energy Commission; the Ministry of Science and Higher Education and the National Science Centre, Poland; the Fundação para a Ciência e a Tecnologia, Portugal; JINR, Dubna; the Ministry of Education and Science of the Russian Federation, the Federal Agency of Atomic Energy of the Russian Federation, Russian Academy of Sciences, and the Russian Foundation for Basic Research; the Ministry of Education, Science and Technological Development of Serbia; the Secretaría de Estado de Investigación, Desarrollo e Innovación and Programa Consolider-Ingenio 2010, Spain; the Swiss Funding Agencies (ETH Board, ETH Zurich, PSI, SNF, UniZH, Canton Zurich, and SER); the National Science Council, Taipei; the Thailand Center of Excellence in Physics, the Institute for the Promotion of Teaching Science and Technology of Thailand, Special Task Force for Activating Research and the National Science and Technology Development Agency of Thailand; the Scientific and Technical Research Council of Turkey, and Turkish

Atomic Energy Authority; the Science and Technology Facilities Council, UK; the US Department of Energy, and the US National Science Foundation.

Individuals have received support from the Marie-Curie programme and the European Research Council and EPLANET (European Union); the Leventis Foundation; the A. P. Sloan Foundation; the Alexander von Humboldt Foundation; the Belgian Federal Science Policy Office; the Fonds pour la Formation à la Recherche dans l'Industrie et dans l'Agriculture (FRIA-Belgium); the Agentschap voor Innovatie door Wetenschap en Technologie (IWT-Belgium); the Ministry of Education, Youth and Sports (MEYS) of Czech Republic; the Council of Science and Industrial Research, India; the Compagnia di San Paolo (Torino); the HOMING PLUS programme of Foundation for Polish Science, cofinanced by EU, Regional Development Fund; and the Thalis and Aristeia programmes cofinanced by EU-ESF and the Greek NSRF.

References

[1] G. Mahlon and S. J. Parke, "Single top quark production at the LHC: Understanding spin", *Phys. Lett.* **B476** (2000) 323, doi:10.1016/S0370-2693(00)00149-0, arXiv:hep-ph/9912458.

[2] M. Jezabek and J. H. Kuhn, "V-A tests through leptons from polarised top quarks", *Phys. Lett.* **B329** (1994) 317, doi:10.1016/0370-2693(94)90779-X, arXiv:hep-ph/9403366.

[3] J. Aguilar-Saavedra and J. Bernabeu, "W polarisation beyond helicity fractions in top quark decays", *Nucl. Phys.* **B840** (2010) 349, doi:10.1016/j.nuclphysb.2010.07.012, arXiv:1005.5382.

[4] J. Aguilar-Saavedra, "Single top quark production at LHC with anomalous Wtb couplings", *Nucl. Phys.* **B804** (2008) 160, doi:10.1016/j.nuclphysb.2008.06.013, arXiv:0803.3810.

[5] J. Aguilar-Saavedra, "A minimal set of top anomalous couplings", *Nucl. Phys.* **B812** (2009) 181, doi:10.1016/j.nuclphysb.2008.12.012, arXiv:0811.3842.

[6] F. Bach and T. Ohl, "Anomalous top couplings at hadron colliders revisited", *Phys. Rev.* **D86** (2012) 114026, doi:10.1103/PhysRevD.86.114026, arXiv:1209.4564.

[7] CDF Collaboration, "The Measurement of Single-Top Polarization with 3.2 fb^{-1}", Conference Note CDF/PUB/TOP/PUBLIC/9920, FNAL, 2009.

[8] CMS Collaboration, "The CMS experiment at the CERN LHC", *JINST* **3** (2008) S08004, doi:10.1088/1748-0221/3/08/S08004.

[9] CMS Collaboration, "Particle–Flow Event Reconstruction in CMS and Performance for Jets, Taus, and $\not{E}_T$", CMS Physics Analysis Summary CMS-PAS-PFT-09-001, 2009.

[10] CMS Collaboration, "Commissioning of the Particle-flow Event Reconstruction with the first LHC collisions recorded in the CMS detector", CMS Physics Analysis Summary CMS-PAS-PFT-10-001, 2010.

[11] CMS Collaboration, "CMS Luminosity Based on Pixel Cluster Counting - Summer 2013 Update", Technical Report CMS-PAS-LUM-13-001, 2013.

[12] S. Alioli, P. Nason, C. Oleari, and E. Re, "A general framework for implementing NLO calculations in shower Monte Carlo programs: the POWHEG BOX", *JHEP* **06** (2010) 043, doi:10.1007/JHEP06(2010)043, arXiv:1002.2581.

[13] S. Alioli, P. Nason, C. Oleari, and E. Re, "NLO single-top production matched with shower in POWHEG: s- and t-channel contributions", *JHEP* **09** (2009) 111, doi:10.1088/1126-6708/2009/09/111, arXiv:0907.4076.

[14] S. Frixione, P. Nason, and C. Oleari, "Matching NLO QCD computations with Parton Shower simulations: the POWHEG method", *JHEP* **0711** (2007) 070, doi:10.1088/1126-6708/2007/11/070, arXiv:0709.2092.

[15] T. Sjöstrand, S. Mrenna, and P. Z. Skands, "PYTHIA 6.4 physics and manual", *JHEP* **0605** (2006) 026, doi:10.1088/1126-6708/2006/05/026, arXiv:hep-ph/0603175.

[16] S. Jadach, J. H. Kuhn, and Z. Was, "TAUOLA: A library of Monte Carlo programs to simulate decays of polarized τ leptons", *Comput. Phys. Commun.* **64** (1990) 275, doi:10.1016/0010-4655(91)90038-M.

[17] J. Alwall et al., "The automated computation of tree-level and next-to-leading order differential cross sections, and their matching to parton shower simulations", *JHEP* **1407** (2014) 079, doi:10.1007/JHEP07(2014)079, arXiv:1405.0301.

[18] T. Sjstrand et al., "An Introduction to PYTHIA 8.2", *Comput. Phys. Commun.* **191** (2015) 159, doi:10.1016/j.cpc.2015.01.024, arXiv:1410.3012.

[19] CompHEP Collaboration, "CompHEP 4.4 – automatic computations from Lagrangians to events", *Nucl. Instrum. Meth.* **A534** (2004) 250, doi:10.1016/j.nima.2004.07.096, arXiv:hep-ph/0403113.

[20] E. E. Boos et al., "Method for simulating electroweak top-quark production events in the NLO approximation: SingleTop event generator", *Phys. Atom. Nucl.* **69** (2006) 1317, doi:10.1134/S1063778806080084. [Yad. Fiz.69,1352(2006)].

[21] M. L. Mangano, M. Moretti, F. Piccinini, and M. Treccani, "Matching matrix elements and shower evolution for top-quark production in hadronic collisions", *JHEP* **01** (2007) 013, doi:10.1088/1126-6708/2007/01/013, arXiv:hep-ph/0611129.

[22] J. Alwall et al., "Comparative study of various algorithms for the merging of parton showers and matrix elements in hadronic collisions", *Eur. Phys. J.* **C53** (2008) 473, doi:10.1140/epjc/s10052-007-0490-5, arXiv:0706.2569.

[23] S. Hoche, F. Krauss, M. Schonherr, and F. Siegert, "Automating the POWHEG method in SHERPA", *JHEP* **1104** (2011) 024, doi:10.1007/JHEP04(2011)024, arXiv:1008.5399.

[24] S. Hoeche, F. Krauss, M. Schonherr, and F. Siegert, "W+n-jet Predictions at the Large Hadron Collider at Next-to-Leading Order Matched with a Parton Shower", *Phys. Rev. Lett.* **110** (2013) 052001, doi:10.1103/PhysRevLett.110.052001, arXiv:1201.5882.

[25] N. Kidonakis, "Differential and total cross sections for top pair and single top production", in *Proceedings, 20th International Workshop on Deep-Inelastic Scattering and Related Subjects (DIS 2012)*, p. 831. 2012. arXiv:1205.3453. [,831(2012)]. doi:10.3204/DESY-PROC-2012-02/251.

[26] M. Czakon and A. Mitov, "Top++: A program for the calculation of the top-pair cross-section at hadron colliders", *Comput. Phys. Commun.* **185** (2014) 2930, doi:10.1016/j.cpc.2014.06.021, arXiv:1112.5675.

[27] R. Gavin, Y. Li, F. Petriello, and S. Quackenbush, "FEWZ 2.0: A code for hadronic Z production at next-to-next-to-leading order", arXiv:1011.3540.

[28] J. M. Campbell and R. Ellis, "MCFM for the Tevatron and the LHC", *Nucl. Phys. Proc. Suppl.* **205-206** (2010) 10, doi:10.1016/j.nuclphysbps.2010.08.011, arXiv:1007.3492.

[29] GEANT4 Collaboration, "GEANT4 – a simulation toolkit", *Nucl. Instrum. Meth.* **A506** (2003) 250, doi:10.1016/S0168-9002(03)01368-8.

[30] CMS Collaboration, "Measurement of the single-top-quark t-channel cross section in pp collisions at $\sqrt{s} = 7$ TeV", *JHEP* **1212** (2012) 035, doi:10.1007/JHEP12(2012)035, arXiv:1209.4533.

[31] M. Cacciari, G. P. Salam, and G. Soyez, "The anti-k_t jet clustering algorithm", *JHEP* **04** (2008) 063, doi:10.1088/1126-6708/2008/04/063, arXiv:0802.1189.

[32] M. Cacciari, G. P. Salam, and G. Soyez, "FastJet user manual", *Eur. Phys. J.* **C72** (2012) 1896, doi:10.1140/epjc/s10052-012-1896-2, arXiv:1111.6097.

[33] CMS Collaboration, "Performance of b tagging at $\sqrt{s}$ =8 TeV in multijet, $t\bar{t}$ and boosted topology events", CMS Physics Analysis Summary CMS-PAS-BTV-13-001, 2013.

[34] CMS Collaboration, "Measurement of the t-channel single top quark production cross section in pp collisions at $\sqrt{s} = 7$ TeV", *Phys. Rev. Lett.* **107** (2011) 091802, doi:10.1103/PhysRevLett.107.091802, arXiv:1106.3052.

[35] CMS Collaboration, "Single Muon efficiencies in 2012 Data", Technical Report CMS-DP-2013-009, 2013.

[36] CMS Collaboration, "Determination of jet energy calibration and transverse momentum resolution in CMS", *JINST* **6** (2011) P11002, doi:10.1088/1748-0221/6/11/P11002, arXiv:1107.4277.

[37] T. Gleisberg et al., "Event generation with SHERPA 1.1", *JHEP* **0902** (2009) 007, doi:10.1088/1126-6708/2009/02/007, arXiv:0811.4622.

[38] CMS Collaboration, "Measurement of differential top-quark pair production cross sections in pp collisions at $\sqrt{s} = 7$ TeV", *Eur. Phys. J.* **C73** (2013) 2339, doi:10.1140/epjc/s10052-013-2339-4, arXiv:1211.2220.

[39] CMS Collaboration, "Measurement of the Differential Cross Section for Top Quark Pair Production in pp Collisions at $\sqrt{s}$ = 8 TeV", arXiv:1505.04480.

[40] V. Blobel, "An Unfolding method for high-energy physics experiments", in *Advanced statistical techniques in particle physics. Proceedings, Conference, Durham, UK, March 18-22, 2002*, p. 258. 2002. arXiv:hep-ex/0208022.

[41] CMS Collaboration, "Measurement of the charge asymmetry in top-quark pair production in proton-proton collisions at $\sqrt{s} = 7$ TeV", *Phys. Lett.* **B709** (2012) 28, doi:10.1016/j.physletb.2012.01.078, arXiv:1112.5100.

[42] H.-L. Lai et al., "New parton distributions for collider physics", *Phys. Rev.* **D82** (2010) 074024, doi:10.1103/PhysRevD.82.074024, arXiv:hep-ph/10072241.

[43] A. D. Martin et al., "Extended Parameterisations for MSTW PDFs and their effect on Lepton Charge Asymmetry from W Decays", *Eur. Phys. J.* **C73** (2013), no. 2, 2318, doi:10.1140/epjc/s10052-013-2318-9, arXiv:1211.1215.

[44] R. D. Ball et al., "Parton distributions with LHC data", *Nucl. Phys.* **B867** (2013) 244, doi:10.1016/j.nuclphysb.2012.10.003, arXiv:1207.1303.

[45] M. R. Whalley, D. Bourilkov, and R. C. Group, "The Les Houches accord PDFs (LHAPDF) and LHAGLUE", in *HERA and the LHC: A Workshop on the implications of HERA for LHC physics. Proceedings, Part B*. 2005. arXiv:hep-ph/0508110.

[46] The ATLAS, CDF, CMS and D0 Collaborations, "First combination of Tevatron and LHC measurements of the top-quark mass", arXiv:1403.4427.